Physics of polymorphic transitions in CeRuSn

J. Fikáček,* J. Prokleška, M. Míšek, J. Custers, S. Daniš, J. Prchal, and V. Sechovský
Faculty of Mathematics and Physics, Charles University in Prague, Ke Karlovu 5, 121 16 Prague 2, Czech Republic

I. Císařová
Department of Inorganic Chemistry, Faculty of Science, Charles University in Prague, Hlavova 8, 128 43 Prague 2, Czech Republic
(Received 9 May 2012; published 13 August 2012)

We report a detailed study of the polymorphic transitions in ternary stannide CeRuSn on high quality single crystals through a combination of x-ray diffraction experiments conducted at 300, 275, and 120 K, and measurements of the thermal expansion, magnetization, and resistivity, along main crystallographic axes. In addition, the transition was followed as a function of pressure up to 0.8 GPa. The present x-ray diffraction data show that the room temperature polymorph consists of the lattice doubled along the c axis with respect to the CeCoAl-type structure consistent with previous reports. Upon cooling, the compound undergoes two successive transitions, first to a quintuple (∼290 K) and than to a triple CeCoAl superstructure at ∼225 K. The transitions are accompanied by a tremendous volume change due to a strong shrinking of the lattice along the c axis, which is clearly observed in thermal expansion. We advance arguments that the volume collapse originates from an increasing number of crystallographically inequivalent Ce sites and the change of ratio between the short and long Ce–Ru bonds. The observed properties of the polymorphic transition in CeRuSn are reminiscent of the $\gamma \rightarrow \alpha$ transition in elementary cerium, suggesting that similar physics, i.e., a Kondo influenced transition and strong lattice vibrations, might be the driving forces.

DOI: 10.1103/PhysRevB.86.054108 PACS number(s): 61.50.Ks, 71.27.+a, 81.30.Hd, 62.50.−p

I. INTRODUCTION

The $4f$ electron in cerium is energetically weakly bound despite the fact that it resides deep within the core of the atom. This is due to the relatively extended nature of the $4f$ wave function. Strong correlations between the Ce $4f$ electron and hybridization between the $4f$ state with those of the ligand states arise in Ce compounds and hence the local environment of the Ce atom dictates whether this electron will remain bound within the core (Ce^{3+} state), join the spatially extended valence electrons (Ce^{4+} state), or reside with certain probability in each. In the last case, the atom is said to be in an "intermediate valent" state with fluctuating charge occupancy of the $4f$ shell state.[1–4] The fragile character of the $4f$ electron due to its sensitivity on interatomic distances, as this determines the hybridization strength, is capitalized on for example investigating quantum critical phenomena, where by either applying hydrostatic pressure or chemical substitution the unit-cell volume shrinks or expands with the result that ground state of the material under investigation changes.[5]

Knowledge about the electronic structure and understanding its relation to the physical properties observed in intermetallics, and in particular rare earth based compounds, is an ambitious undertaking in condensed matter research. Investigation by varying the properties utilizing pressure or chemical substitution is one way. In addition, some compounds exist in more than one crystallographic structure.[6] By means of pressure and/or temperature it is possible to convey one into the other reversibly. Such polymorphic transitions allow for comparative study.[7] The chemical composition is retained but bonds of the individual atoms and, therefore, the overall electronic structure and related physical properties can differ significantly. An example is $LaIr_2Si_2$. Polymorphism of $LaIr_2Si_2$ between a high-temperature phase of the primitive tetragonal $CaBe_2Ge_2$-type structure and a low-temperature phase of the body-centered tetragonal $ThCr_2Si_2$-type structure has been demonstrated by Braun *et al.*[8] Notably, the high-temperature modification displays superconductivity below 1.6 K, while the low-temperature phase is normal down to 1 K.

The polymorphic isostructural γ (fcc) $\rightarrow$ α (fcc) transition in elementary cerium[9] is illustrative for the difficulty in understanding the complexity between "chemical bonds," "physical properties," and "structural transition" especially in materials with electrons near the boundary between itinerant and localized behavior.[10] The transition involves a large volume collapse of ∼17% at room temperature and pressure ∼0.8 GPa. A general consensus exists to attribute the transition to an instability of the Ce $4f$ electron. However, Johansson[11] explained the $\gamma \rightarrow \alpha$ transition as a sort of Mott transition in which the localized $4f$ electrons in the γ phase become itinerant and participate in bonding in the lower volume α phase. This model continues to compete with the Kondo-volume-collapse scenario,[12,13] which assumes that the $4f$ electron is localized in both the γ and α phases. The loss of magnetic moment in the α phase results from screening of the moments by the surrounding conduction electrons. To complicate, the latest neutron and x-ray diffraction studies acknowledge the importance of lattice vibrations as well.[14,15]

In many aspects the recently observed polymorphic transition in the equiatomic stannide CeRuSn seems to have much in common with the $\gamma \rightarrow \alpha$ transition in cerium. CeRuSn at room temperature crystallizes in a superstructure modification of the monoclinic CeCoAl-type crystal structure (new monoclinic type, space group $C2/m$) with lattice parameters $a =$ 11.561(4) Å, $b = 4.759(2)$ Å, $c = 10.233(4)$ Å, and $\beta =$ $102.89(3)^\circ$.[16] As a consequence of this doubling of the original CeCoAl unit cell along the c axis, the compound possesses two crystallographically independent cerium sites labeled

Ce1 and Ce2. Although topology of both cerium sites is identical, five rhodium, six tin, and six cerium atoms in the coordination shell, the tiny changes in interatomic distances, most notably the Ce–Ru bonds (Ce1–Ru: ranging from 2.33 to 2.46 Å; Ce2–Ru: ranging from 2.88 to 2.91 Å) result in Ce1 being in intermediate valent state while Ce2 shows strong localization of the f electron as suggested by magnetic susceptibility experiments.[16,17] This presumption is borne out by electronic structure calculations[18] and proven by x-ray absorption near-edge structures (XANES) data.[19] Latest yields average valencies of 3.18 for Ce1 and Ce2.

The polymorphic transition in CeRuSn sets in just below room temperature at ∼290 K and is completed at around ∼160 K upon cooling. The reverse transformation occurs on heating with ∼170 K and ∼320 K as the onset and end temperatures, respectively. Initial measurements of magnetic susceptibility, specific heat, thermopower, and resistivity were performed on polycrystalline samples.[17] The transformation was smeared out and manifested a broad hysteresis with a cusplike structure in resistivity, a steplike decrease of the susceptibility, a broad hump in the specific heat, and a strong increase in thermopower. A detailed analysis of the transition by means of synchrotron x-ray diffraction experiments on a single crystal revealed that the room temperature phase is replaced by a set of close to commensurate modulations along the c axis, namely quintupling (∼290 K) and (dominant) quadrupling (below 210 K) before finalizing (∼180 K) in an ill-defined modulated ground state, which is close to a tripling of the basic monoclinic CeCoAl-type structure.[19]

The present work gives a detailed examination of the physical properties of the polymorphic transition of CeRuSn. For this purpose, measurements were performed on high quality single crystals. The lower amount of crystal lattice defects, absence of grain boundaries, and the ability to perform experiments along specific crystallographic orientations allows us to resolve details related to the transition and to attribute those signatures in the experiments to the respective modulation in the structure.

II. EXPERIMENTAL DETAILS

1. Sample preparation

Single crystals of CeRuSn were prepared in two stages. First a polycrystalline button of the nominal 1:1:1 stoichiometry was synthesized using elements of purity 3N Ce (Ce from Alpha Aesar which was additionally purified by solid state electrotransport technique[20]), 4N Ru, and 5N Sn as starting materials. The reaction of the stoichiometric mixture of the elements was performed on a water-cooled copper crucible in a monoarc furnace under 6N argon atmosphere. The mass difference before and after the reaction was negligible (<0.1%). The crystal was then grown utilizing a modified Czochralski technique; the button was remelted in a triarc furnace under 6N argon protection atmosphere and a tungsten rod was used as a seed.

The quality of the single crystal was checked by x-ray Laue backscattering, which was also used for orienting the crystals later on. The chemical composition was verified employing a Tescan Mira I LMH scanning electron microscope (SEM). The instrument is equipped with a Bruker AXS energy dispersive x-ray detector (EDX). Within the accuracy of the device, no impurity phases were resolved and the measurement confirmed the correct 1:1:1 stoichiometry.

Afterwards, the crystal was cut for further analysis. One piece was pulverized and examined at room temperature by means of powder x-ray diffraction (Bruker D8 Advance diffractometer with Cu K_α radiation with $\lambda = 1.5405$ Å). The obtained diffraction patterns were refined by Rietveld analysis using FULLPROF.[21] The analysis confirmed the CeCoAl superstructure and the corresponding lattice parameters agreed well with those values reported in literature.[16] The other piece of the crystal was annealed at 700 °C for one week in vacuum ($p = 1 \times 10^{-6}$ mbar) in order to improve homogeneity.

2. Experimental setup

From the annealed single crystal a small piece was cut for investigating the crystal structure by x rays at defined temperatures. Therefore, the approximately $0.1 \times 0.1 \times 0.1$ mm^3 piece was placed inside a Lindemann capillary. The capillary itself was mounted into a Bruker Apex II diffractometer with Mo K_α radiation ($\lambda = 0.71073$ Å). In order to reach lower temperatures, the capillary was inserted into a flow of cold nitrogen gas. The crystal structure was resolved by direct methods[22] and adjacent refinement was done by full matrix least squares based on F^2.

Bulk properties were retrieved employing standard equipment. The magnetization was measured in a MPMS7 (Quantum Design). Data were collected in the temperature range from 1.8 to 350 K and in fields up to 7 T. Resistivity, Hall resistivity, thermopower, and thermal conductivity were measured in a PPMS14 (Quantum Design) using the respective optional accessories of the device. The temperature was varied between 1.8 and 350 K and magnetic fields up to 14 T were applied. The resistivity was measured using standard four-point technique. In order to reduce contact resistance, 25-μm-diameter Au wires were spot welded onto the sample. Measurements of the resistivity were performed at ambient and hydrostatic pressure. For the later, the PPMS device was used only to control temperature. The sample was loaded into a double cylinder CuBe/NiCrAl pressure cell. Daphne 7373 oil was used as pressure medium and the applied pressure was determined at room temperature utilizing a manganin manometer.

The thermal expansion was measured in a temperature interval of 180–340 K. The sample was built into a miniature capacitance cell.[23] The capacity was read out by an Andeen Hagerling 2500A capacitance bridge. The cell was inserted into a PPMS whose controlling was used to set temperature.

Most of the experiments were conducted on both the as cast and the annealed single crystals. The quality of the crystals improved considerably by annealing. The resistivity behavior of the as cast crystals to some extent resembled the results of the polycrystalline sample presented in earlier work[17] that is a single broad hysteresis, which differs in detail depending on the current direction with respect to the crystallographic axis. On the contrary the annealed crystals exhibit two sharp transitions evident for two distinct transitions as will be discussed below. In addition, differences in the hysteresis of each of the transitions could be resolved. Results presented in

this paper were obtained on the annealed crystals. The bulk properties were measured with respect to the three principal crystallographic axes. Data shown have been collected on two batches. The resistivity and susceptibility experiments were performed on batch I, while for thermal expansion a piece from batch II was used. Hence slight differences in the respective transition temperatures are observed, which we attribute to sample dependencies.

III. RESULTS

A. Measurement of bulk properties

Figure 1 depicts the temperature dependence of the scaled electrical resistivity $\rho/\rho_{1.8\,\mathrm{K}}$ for current applied along the a, b, and c axis. The inset shows the full temperature range. The different corresponding values for $\rho(T)$ document anisotropy of the electronic transport in CeRuSn. Yielding $\rho_{300\,\mathrm{K}}/\rho_{1.8\,\mathrm{K}} \sim 18$ (for $I \parallel a$) comparing to only $\sim$1.75 for a polycrystalline sample proves the high quality of our single crystals. More remarkably, the observed behavior in resistivity differs significantly from previously published work on a polycrystalline sample.[17] Cooling down the sample (solid lines in Fig. 1) from above room temperature, the resistivity undergoes a sharp steplike increase by about 7% just below 290 K. The anomaly, indicated by $T_{\mathrm{U}}^{\mathrm{c}}$ in the main panel, is clearly seen in all applied current directions while absent in the polycrystalline sample. Below 225 K, a second transition emerges marked by $T_{\mathrm{L}}^{\mathrm{c}}$, and the resistivity seems to fall back onto the original curve from before the first transition ($I \parallel c$ and a). The transition is weakly pronounced for $I \parallel b$ while decrease of the resistivity is only a fraction of the increase at $T_{\mathrm{U}}^{\mathrm{c}}$. Interestingly, this $T_{\mathrm{L}}^{\mathrm{c}}$ transition, although slightly shifted towards lower temperatures, is observed in the

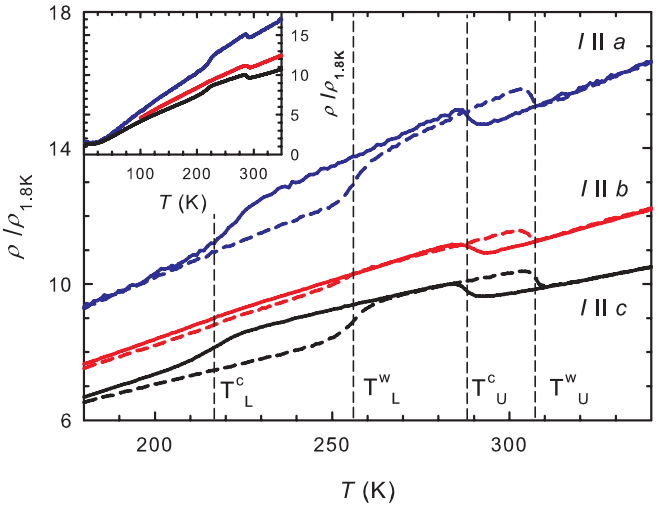

FIG. 1. (Color online) Temperature dependences of the relative resistivity $\rho(T)/\rho_{1.8\,\mathrm{K}}$ of CeRuSn measured with current applied along the three principal crystallographic directions for cooling (solid lines) and warming (short-dashed lines). The main panel focuses on the temperature range the discussed transitions take place. The vertical dashed lines mark the estimated transition temperatures $T_{\mathrm{U}}^{\mathrm{c}}$, $T_{\mathrm{L}}^{\mathrm{c}}$, $T_{\mathrm{L}}^{\mathrm{w}}$, and $T_{\mathrm{U}}^{\mathrm{w}}$ (see text). The inset shows the whole temperature range of the experiment for cooling regime.

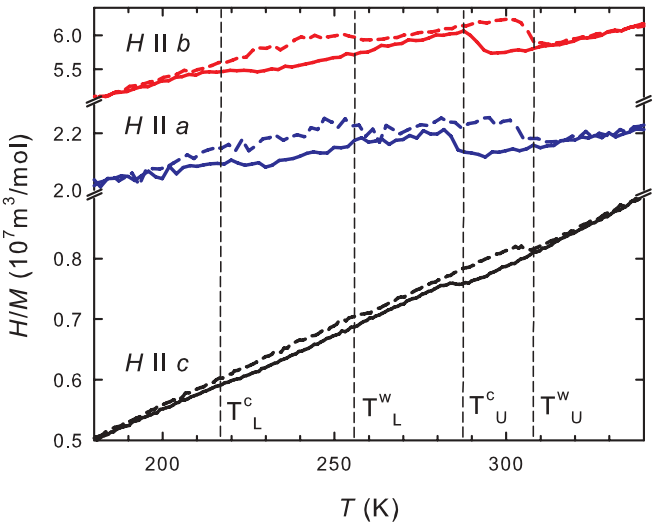

FIG. 2. (Color online) Inverse magnetic susceptibility $\chi^{-1}(T) = H/M(T)$ of CeRuSn in magnetic field applied along the a, b, and c axis in the temperature interval of interest. Solid (short-dashed) lines denote measurements in cooling down (warming up). The applied magnetic field was 1 T for $H \parallel a$ and $H \parallel c$ and 7 T for $H \parallel b$. The vertical lines are guides to the eye illustrating the estimated transition temperatures $T_{\mathrm{U}}^{\mathrm{c}}$, $T_{\mathrm{L}}^{\mathrm{c}}$, $T_{\mathrm{L}}^{\mathrm{w}}$, and $T_{\mathrm{U}}^{\mathrm{w}}$ from temperatures of the resistivity anomalies. Mind the breaks in the scale on the vertical axis.

polycrystal as well. However, contrary to our data, resistivity increases. Below 3 K, resistivity reveals a third anomaly, which can be attributed to the onset of antiferromagnetic ordering reported earlier.[17] In the following, discussion on the antiferromagnetic order is omitted and focus is entirely on the relevant temperature range of $T_{\mathrm{U}}^{\mathrm{c}}$ and $T_{\mathrm{L}}^{\mathrm{c}}$.

Upon warming up (dashed lines in Fig. 1), both the lower, $T_{\mathrm{L}}^{\mathrm{w}}$ $\sim$256 K, and upper, $T_{\mathrm{U}}^{\mathrm{w}}$ $\sim$307 K, transitions of $\rho(T)$ preserve shape and size of the step. However, they are observed at much higher temperatures than their corresponding anomalies when cooling down, i.e., exhibiting a large temperature hysteresis. In comparison, hysteresis of the lower-temperature transition yields $T_{\mathrm{L}}^{\mathrm{w}} - T_{\mathrm{L}}^{\mathrm{c}} \sim 40$ K almost double the hysteresis of the upper-temperature transition $T_{\mathrm{U}}^{\mathrm{w}} - T_{\mathrm{U}}^{\mathrm{c}} \sim 20$ K. These remarkable features in CeRuSn remain intact even in magnetic fields up to 14 T.

Figure 2 plots the temperature dependence (solid lines refer to cooling down, dashed lines for warming up sequence) of the inverse dc magnetic susceptibility, χ^{-1}, in fields applied along the principal crystallographic axes. The magnetic susceptibility is strongly anisotropic apparently due to the influence of the very low-symmetry crystal electric field (CEF) on the orbitals of the Ce ion. The transitions at $T_{\mathrm{U}}^{\mathrm{c}}$ and $T_{\mathrm{L}}^{\mathrm{c}}$ when cooling down, and $T_{\mathrm{L}}^{\mathrm{w}}$ and $T_{\mathrm{U}}^{\mathrm{w}}$ when warming up, are clearly witnessed by a small negative step in the magnetization, i.e., a positive jump in χ^{-1}. Note that the polycrystalline sample shows only a single step upon cooling at $T \sim 180$ K.[16,17] The lower transitions $T_{\mathrm{L}}^{\mathrm{c}}$ and $T_{\mathrm{L}}^{\mathrm{w}}$ are much weaker than the upper ones.

Short temperature intervals that are above $T_{\mathrm{U}}^{\mathrm{c}}$ and between $T_{\mathrm{U}}^{\mathrm{c}}$ and $T_{\mathrm{L}}^{\mathrm{c}}$ prevent a meaningful qualitative analysis of the temperature dependence of each of the separate paramagnetic phases. Quantitatively, assuming the effective moment remains conserved across the transitions, a reasonable assumption

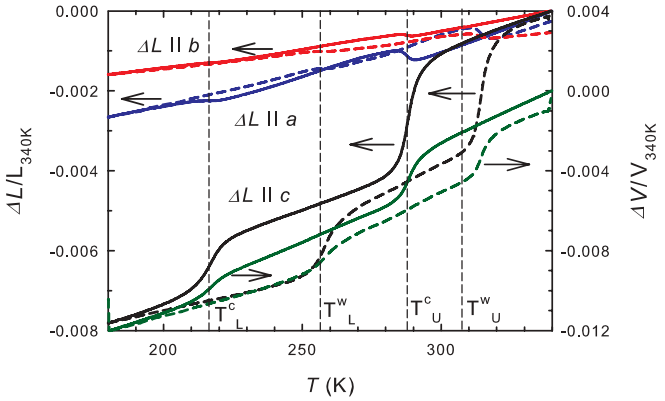

FIG. 3. (Color online) Temperature evolution of the relative change of length $\Delta L/L_{340\,\mathrm{K}}$ (left axis) resolved for each of the principal crystallographic directions when the sample was in cool down (solid line) and warm up run (short-dashed line) through the transitions. On the right axis, the calculated relative volume change $V/V_{340\,\mathrm{K}}$ for cooling (solid line) and warming (short-dashed line) is depicted.

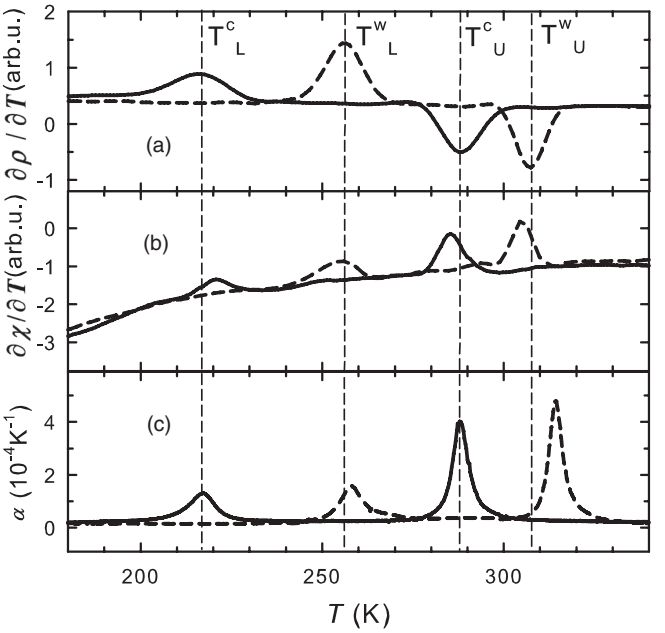

FIG. 4. Comparative plot of the temperature dependences of (a) the temperature derivative of the electrical resistivity $\partial\rho/\partial T$ for $I \parallel c$, (b) the temperature derivative of the magnetic susceptibility $\partial\chi/\partial T$ with $H \parallel c$, and (c) the linear thermal expansion coefficient $\alpha(T)$ along the c axis. Solid (short-dashed) lines show data taken when cooling down (warming up) the sample. The vertical lines are guides to the eye illustrating the estimated transition temperatures $T_{\mathrm{U}}^{\mathrm{c}}$, $T_{\mathrm{L}}^{\mathrm{c}}$, $T_{\mathrm{L}}^{\mathrm{w}}$, and $T_{\mathrm{U}}^{\mathrm{w}}$, respectively, from temperatures of the resistivity anomalies.

recalling that XANES unveil no change in Ce valency;[16] the change in $\chi(T)$ implies a shift of the paramagnetic Curie temperatures towards larger negative values for each field direction objecting statements on the polycrystalline sample.[16]

Detailed dilatometric measurements performed on a well-defined single crystal provide important information on the evolution of the lattice parameters. The thermal expansion was measured along each of the three principal crystallographic directions. As presented in Fig. 3, two steps are observed along each of the axes at similar temperatures to the anomalies recorded in $\rho(T)$ and $\chi(T)$. When cooling (solid lines in Fig. 3) from room temperature, the crystal contracts considerably along the c axis by almost 0.8% between 340 and 180 K. Contrary, the tiny positive jumps disclosed for a and b directions represent a very small expansion of a and nearly negligible increase of the lattice parameter b, respectively. Consequently, the volume changes at $T_{\mathrm{U}}^{\mathrm{c}}$ and $T_{\mathrm{L}}^{\mathrm{c}}$ express mainly the c axis behavior, i.e., the crystal shrinks in two steps with decreasing temperature. The corresponding reverse transitions appear at $T_{\mathrm{L}}^{\mathrm{w}}$ and $T_{\mathrm{U}}^{\mathrm{w}}$ corroborating the hysteretic behavior of the phases as inferred by resistivity and magnetization experiments already.

In Fig. 4, a comparison of the temperatures of the anomalies disclosed in aforementioned bulk experiments is made. To visualize the location of the transition more clearly, the temperature derivative of the resistivity ($\partial\rho/\partial T$), dc magnetic susceptibility ($\partial\chi/\partial T$), and thermal expansion coefficient (α) along the c axis are displayed. The maxima in ($\partial\rho/\partial T$) and (α) well coincide except for the $T_{\mathrm{U}}^{\mathrm{w}}$ transition. This difference likely arose because a sample from batch II had been used, as mentioned in Sec. II.

B. X-ray single crystal study of polymorphs

The presented results on resistivity, magnetization, and thermal expansion conflict in many ways with earlier studies.[16,17] Moreover, it was mentioned in the Introduction that in CeRuSn several polymorphic transitions gradually emerged on cooling, which gave rise to additional reflections in the diffraction patterns obtained by synchrotron experiment.[19] Those superstructure reflections can be described by nearly inverse-integer folded propagation vectors having nonzero c components only. The first transition takes place just below room temperature, changing from a $^1/_2$- to a $^1/_5$-like modulation. Upon cooling, these become partially suppressed and replaced by $^1/_4$-like ones, which are dominant at 210 K. Finally, a $^1/_3$-kind modulation develops having the most intensive reflections below 180 K. This one coexists with the aforementioned modulations down to at least 100 K.[19] While $T_{\mathrm{U}}^{\mathrm{c}}$ can be attributed to the first polymorphic transition ($^1/_2 \rightarrow {}^1/_5$) no evidence is found in the data for the structural change $^1/_5 \rightarrow {}^1/_4$, which at least is accepted to manifest in thermal expansion being an extremely sensitive experiment on lattice changes. To anticipate speculations about the structure, a detailed x-ray single crystal diffraction study over the majority of the reciprocal lattice and at defined temperatures was conducted. The following temperature sequence was applied: 300 K, 290 K, 275 K, 120 K, and 200 K matching the regions for determining the structure above $T_{\mathrm{U}}^{\mathrm{c}}$ between $T_{\mathrm{U}}^{\mathrm{c}}$ and $T_{\mathrm{L}}^{\mathrm{c}}$ below $T_{\mathrm{L}}^{\mathrm{c}}$ and below $T_{\mathrm{L}}^{\mathrm{w}}$, respectively.

In all cases, the space group $C2/m$ for the unit cell has been observed. However, the size of the unit cell varies significantly because of formation of superstructures as displayed in Table I. In comparison, the simultaneous changes of the a and b cell parameters are rather negligible and the crystal unit cell size change is related to integer multiplications of the original CeCoAl-type unit along the c axis in agreement with Ref. 19. Within this process, the number of inequivalent Ce lattice sites

TABLE I. Lattice parameters determined from SC x-ray diffraction. The lattice parameters are sorted according to the temperature evolution during our experiment. The last column shows the ratio between Δc_{red} standing for the c axis modified to room temperature size and the room temperature c axis value. It estimates the real change of crystal dimension along the c direction.

T (K)	a (Å)	b (Å)	c (Å)	β (deg)	V (Å^3)	$\Delta c_{\mathrm{red}}/c_{300\ \mathrm{K}}$ (%)
297	11.565(1)	4.7529(5)	10.2299(9)	103.028(2)	547.85(9)	–
290	11.560(3)	4.751(1)	10.227(3)	103.081(7)	547.1(2)	0.028(1)
275	11.576(2)	4.7556(7)	25.454(3)	102.959(4)	1365.6(3)	0.47(1)
120	11.566(2)	4.7477(6)	15.229(2)	103.554(4)	813.0(2)	0.70(2)
200	11.569(2)	4.7505(6)	15.237(2)	103.496(4)	814.3(2)	0.76(2)

in the intermediate (275 K) and low temperature (120, 200 K) phase, respectively, is larger than in the room temperature polymorph (300, 290 K). The structure at 300 K (Fig. 5) is practically identical to that one at 290 K and in accordance to previous reports.[16,19] Upon cooling below the first transition to $T = 275$ K, a tremendous prolongation of the c axis is observed. The resulting superstructure can be described as a quintuple of the CeCoAl subcell with five crystallographically independent cerium sites (see Fig. 5). With further cooling down to 120 K, CeRuSn passes through the second

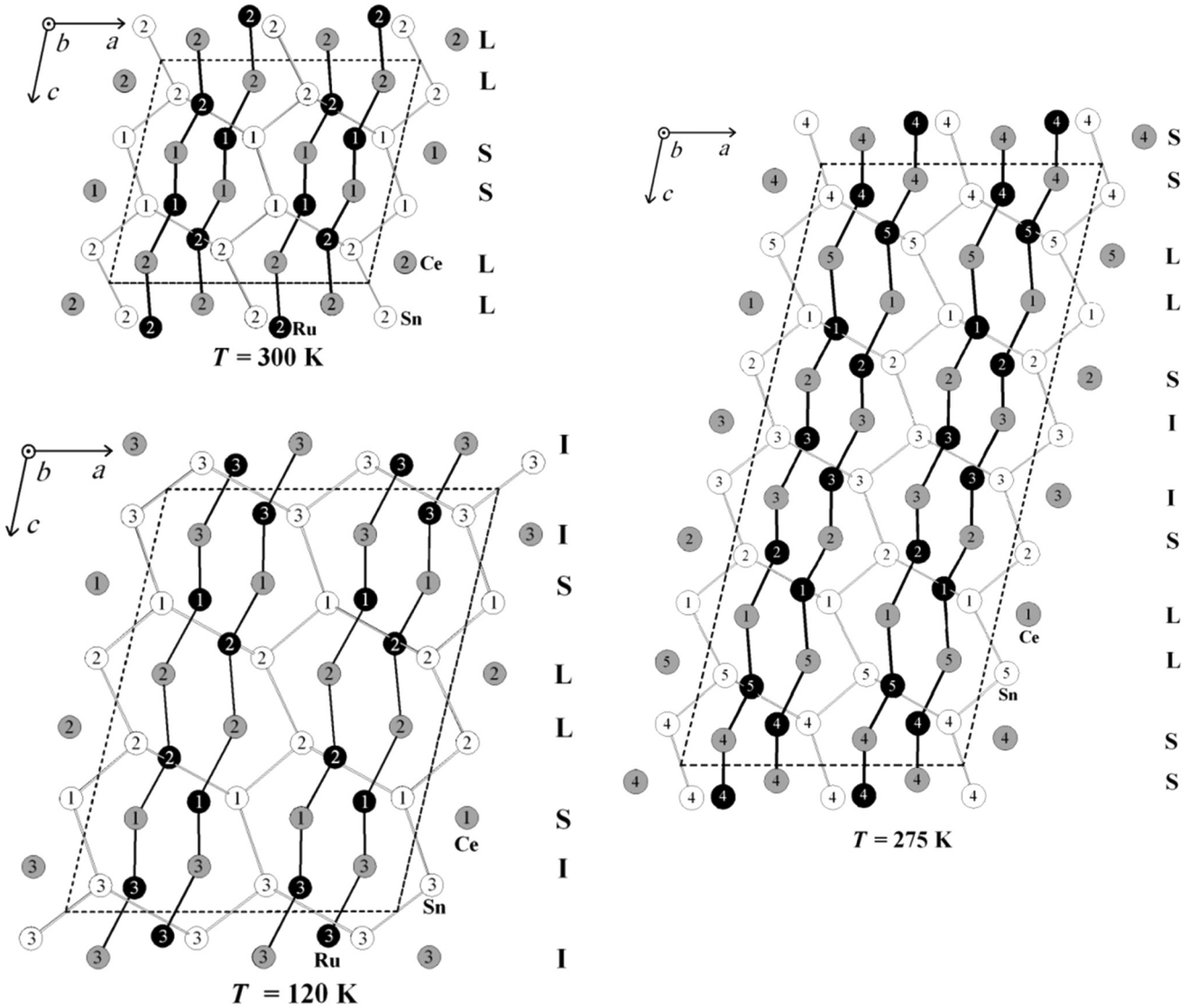

FIG. 5. Illustration of CeRuSn crystal structures above, between, and below the transitions at 300, 275, and 120 K, respectively. For all types of atoms, numbers label two nonequivalent crystallographic sites. Ce sites are additionally marked on the right-hand side by S, L, and I letters according to the similarity of their environment shown in Table II. Black and white lines emphasize the typical Ce–Ru shortest interatomic distances and tin network, respectively. Dashed lines illustrate Bravais unit cells.

TABLE II. Closest ruthenium neighbors of cerium atoms at different temperatures. (*S*), (*L*), and (*I*) denote bond type *short*, *long*, and *intermediate*, respectively (see also text).

$T = 300$ K				$T = 275$ K				$T = 120$ K			
Ce1	2.3277(9)	Ru1	(*S*)	Ce1	2.8882(19)	Ru5	(*L*)	Ce1	2.4325(18)	Ru2	(*S*)
	2.4661(11)	Ru2			2.9247(19)	Ru2			2.4345(18)	Ru3	
Ce2	2.8783(10)	Ru1	(*L*)	Ce2	2.4331(18)	Ru1	(*S*)	Ce2	2.9153(17)	Ru1	(*L*)
	2.9081(10)	Ru2			2.4380(19)	Ru3			2.9257(18)	Ru2	
				Ce3	2.271(2)	Ru2	(*I*)	Ce3	2.2676(17)	Ru1	(*T*)
					2.7575(19)	Ru3			2.7482(17)	Ru3	
				Ce4	2.3219(19)	Ru4	(*S*)				
					2.4779(18)	Ru5					
				Ce5	2.8800(18)	Ru4	(*L*)				
					2.9453(19)	Ru1					

polymorphic transition at T_L^c. The final and only existing structure can be viewed as a tripling of the CeCoAl unit-cell exhibiting three different cerium sites (Fig. 5). The nearest Ce–Ru distances for all phases are summarized in Table II. With closer inspection of the crystallographic parameters, one can see that all the interatomic distances were more or less modified. But the crucial aspect seems to be the increased number of Ce positions with short Ce–Ru pairs (cf. Table III). This explains the *c* axis contraction, since Ce–Ru bonds are oriented almost entirely along this direction and scales the distances along the *c* axis. Calculating the relative change of the average CeCoAl subcell from the obtained lattice parameters yields a shrinking of about 0.47% (between room temperature and 275 K) and 0.70% (between room temperature and 120 K) along the *c* axis, which is in line with the thermal expansion results.

IV. DISCUSSION

Signatures of the polymorphic transitions were presented for resistivity, magnetization, and thermal expansion. We did not show the data on the thermoelectric power, temperature evolution of the Hall effect, and thermal conductivity in which also a steplike structure was observed at T_U^c, T_L^c, T_L^w, and T_U^w. All these findings strongly indicate that the polymorphic transition involves a Fermi surface reconstruction accompanied by a change of the electronic structure. A strong electron-lattice coupling is to be expected. Moreover, as pointed out in the Introduction, because of mutual interplay between electronic structure and interatomic forces, various lattice vibration properties can be expected according to whether the $4f$ moment is localized or in an intermediate state. It was discussed by Mydosh *et al.*[17] that the steplike reduction of the magnetization signals a decrease of the density of states, i.e., change of the electronic structure. However, one might interpret the observed reduction in $\chi(T)$ (see Fig. 2) as manifestation of a sudden (partial) Kondo screening of the localized Ce2 moments in CeRuSn. The slightly higher than expected resistivity values for $I \parallel b$ below T_L^c therefore would be a result of a reduction of conduction electrons involved in screening. Such scenario applies to cerium where lattice vibrations are suggested to play an important role in the Ce $\gamma \rightarrow \alpha$ transition together with spin and charge degrees of freedom.[14]

Speculation about an analogy with elementary cerium are further inspired by hydrostatic pressure experiments on CeRuSn. The upper accessible temperature (380 K) is limited by the properties of the StyCast epoxy used for sealing of the wires in the plug of the pressure cell. In Fig. 6, the resistivity data in arbitrary units are depicted against temperature at ambient and at pressures of $p = 0.4$ and 0.8 GPa. The character of the transitions remains qualitatively the same even at highest applied pressure when they are still observable within the temperature range of the experiment. Interestingly, within the applied pressure range and the resolution of the experiment, T_U^c, T_L^c, T_L^w, and T_U^w increase roughly linearly with an identical rate; see Fig. 7. The slopes of the respective polymorphic transition shift amounts to approximately 125 K/GPa. This linear increase of the transition temperature is reminiscent to the linear shifting of the $\gamma \rightarrow \alpha$ phase line of cerium.[24] Here

TABLE III. Fraction atomic coordinates $^x/_a$, $^y/_b$, and $^z/_c$ at 300 K and 120 K.

$T = 300$ K				$T = 120$ K			
Ce1	0.1396	0	0.4146	Ce1	0.6306	0	0.1075
Ce2	0.1225	0	0.9063	Ce2	0.3567	0	0.2216
				Ce3	0.6226	0	0.4375
Sn1	0.4265	0	0.3469	Sn1	0.0858	0	0.9376
Sn2	0.4043	0	0.8486	Sn2	0.0906	0	0.6008
				Sn3	0.0659	0	0.2688
Ru1	0.1827	0	0.6481	Ru1	0.6784	0	0.2605
Ru2	0.1983	0	0.1973	Ru2	0.2992	0	0.3654
				Ru3	0.3102	0	0.0572

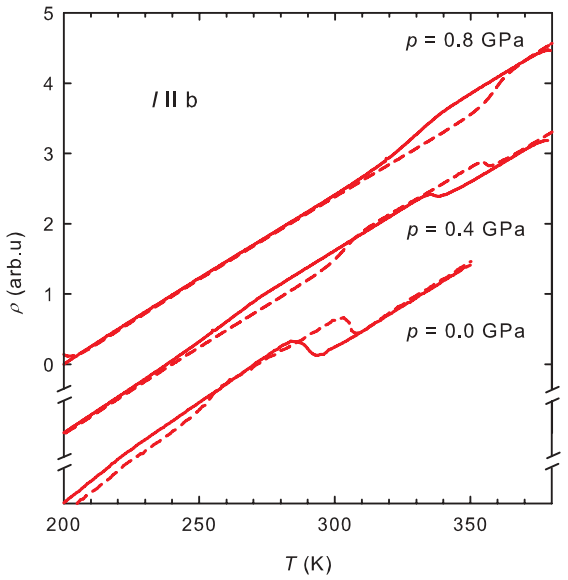

FIG. 6. (Color online) Temperature dependency of the resistivity of CeRuSn at ambient and under hydrostatic pressure $p = 0.4$ GPa and 0.8 GPa. The current is applied along the b axis. Solid (short-dashed) lines show measurements in cooling down (warming up). The curves are shifted for clarity. For $p = 0.8$ GPa, the upper transition is shifted beyond the maximum temperature of our experiment already.

the slope is roughly 250 K/GPa[10] twice the observed rate in CeRuSn.

The results of the structural investigation can be understood as a subsequent annealing and consecutive evolution of polymorph phases. In the determined phases, the cerium position (see Table II) can be divided into three groups—those exhibiting two short (S) Ce–Ru distances (close Ru nearest neighbors), those with two long (L) Ce–Ru distances (far nearest neighbors), and those (I) with one close and one far Ru nearest neighbor (within each group, there is a variation of the Ce–Ru distance across the polymorphs but in comparison to the short-long distance the change is minimal). With this in mind (see Fig. 5), the low temperature structure can be described as *SLLS* base building block (two CeCoAl subcells, same sequence as at room temperature) alternating with the *II* cerium sequence (leading to the tripling of the CeCoAl subcell observed at low temperatures) along the c axis. With increasing temperature, a rearrangement by displacive transformation leads to the extinction of half of the *II* spacers leaving the structure with quintuple CeCoAl subcell (two base blocks, one spacer). Further heating up removes the rest of the *II* spacers and results in the appearance of the base building block at high temperatures. Within this context, the existence of the *II* spacer can be understood as a deformation of the CeCoAl-sized cell driven by cohesion forces in order to stabilize the whole structure. The results of the XANES experiment[19] seem to be in contradiction with the above presented structural data (with decreasing temperature the number of sites with short Ce–Ru distance is increased). However, it is necessary to keep in mind that the dependence of the valence on the Ce–Ru distance is not simple and that there are several different short Ce–Ru distances at lower temperatures. This nonlinearity together with an increased number of crystallographically inequivalent Ce sites and presumable Kondo screening leads to shrinking of the c axis concurrently and to an unchanged overall Ce valence, which is different from the statement[19] that the valence of the Ce ions through the transition remains conserved. Further experiments resolving this issue are desired.

To find the true nature, i.e., the driving mechanism behind the polymorphic transitions is a challenging task for future work. The transitions in CeRuSn show to some extent similarities to the cerium case, which might serve as reference point. In order to enlighten the role of lattice vibrations, inelastic neutron scattering experiments are envisaged.

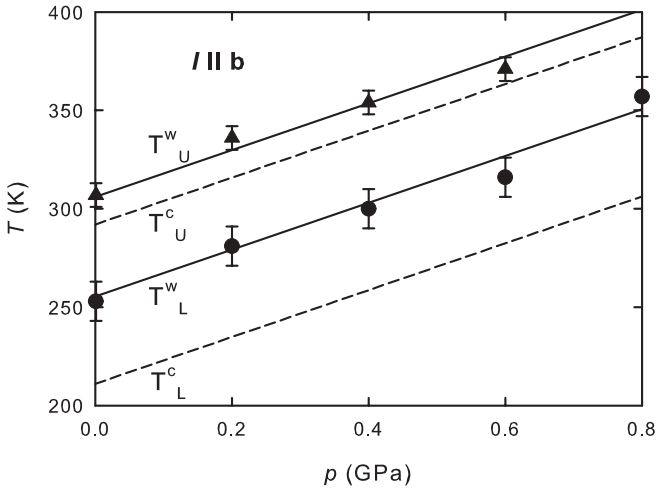

FIG. 7. p-T phase diagram of CeRuSn determined by resistivity experiments under hydrostatic pressure. The full lines are the guides for the eye separating the high-temperature, intermediate, and low-temperature polymorphic phase, for the warming regime. The dashed lines represent the alternative for the cooling regime. In this case, the data are not displayed.

V. SUMMARY

Investigation of the polymorphic transitions by means of resistivity, magnetization, thermal expansion, and x-ray diffraction on single crystals of CeRuSn was carried out. Measurements were conducted along all principal axes. In all physical properties, upon cooling, two subsequent anomalies at $T_U^c \sim 285$ K and $T_L^c \sim 185$ K were detected. These signatures can be attributed to polymorphic transitions, i.e., from the room temperature double CeCoAl-type superstructure to a quintuple at T_U^c and from the quintuple to a triple CeCoAl unit-cell superstructure at the lower transition temperature. The refined superstructures are characterized by an increased number of crystallographically inequivalent Ce sites. Simultaneously, the ratio between the number of short and long Ce–Ru bonds, which are essentially aligned along c direction, is increased. As a consequence, the lattice gradually contracts mainly along the c axis as observed in thermal expansion eliciting an overall shrinking of the sample volume. The transitions exhibit large hysteresis behavior.

The strong response of the polymorphic transitions in transport and magnetic properties infers a close connection

to variations in the electronic structure of CeRuSn. Slight jumps in the magnetization as well as unexpected behavior in resistivity suggest influence of Kondo interaction to play a role in the structural change. Together with lattice vibrations, it might be the driving mechanism behind the polymorphic transitions similar to the one in elementary cerium. This scenario is partially rooted in resistivity data on CeRuSn under hydrostatic pressure revealing an almost linear increase of the transition temperatures upon pressure as had been observed for the $\gamma \rightarrow \alpha$ transition in Ce as well.

ACKNOWLEDGMENTS

This work was supported by the Czech Science Foundation (Project No. 202/09/1027) and Charles University Grants No. GAUK440811 and No. UNCE 11.

*fikacekjan@seznam.cz

[1] J. G. Sereni, J. Less-Common Met. **86**, 287 (1982).
[2] B. Johansson and N. Mårtensson, in *Handbook on the Physics and Chemistry of Rare Earths*, edited by K. A. Gschneider, Jr., L. Eyring, and S. Hütner (Elsevier Science Publishers B. V., Amsterdam, 1987), Chap. 69, p. 361.
[3] D. Malterre, Solid State Commun. **69**, 475 (1989).
[4] P. Fulde, *Electron Correlations in Molecules and Solids*, Vol. 100 of Solid State Science, 3rd. ed. (Springer Verlag, Heidelberg, 1995).
[5] H. v. Löhneysen, A. Rosch, M. Vojta, and P. Wölfle, Rev. Mod. Phys. **79**, 1015 (2007).
[6] See, for example, E. H. El Ghadraoui, J. Y. Pivan, R. Guérin, O. Pena, J. Padiou, and M. Sergent, Mater. Res. Bull. **23**, 1345 (1988).
[7] M. Mihalik, M. Diviš, V. Sechovský, N. Kozlova, J. Freudenberger, N. Stüßer, and A. Hoser, Phys. Rev. B **81**, 174431 (2010).
[8] H. F. Braun, N. Engel, and E. Parthé, Phys. Rev. B **28**, 1389 (1983).
[9] P. W. Bridgman, Proc. Am. Acad. Arts Sci. **76**, 71 (1948).
[10] D. C. Koskenmaki and K. A. Gschneidner, Jr., in *Handbook on the Physics and Chemistry of Rare Earths*, edited by K. A. Gschneidner, Jr. and L. Eyring (Elsevier Science Publishers B. V., Amsterdam, 1978), Chap. 4, p. 337.
[11] B. Johansson, Philos. Mag. **30**, 469 (1974).
[12] J. W. Allen and R. M. Martin, Phys. Rev. Lett. **49**, 1106 (1982).
[13] J. W. Allen and L. Z. Liu, Phys. Rev. B **46**, 5047 (1992).
[14] I.-K. Jeong, T. W. Darling, M. J. Graf, Th. Proffen, R. H. Heffner, Yongjae Lee, T. Vogt, and J. D. Jorgensen, Phys. Rev. Lett. **92**, 105702 (2004).
[15] M. J. Lipp, D. Jackson, H. Cynn, C. Aracne, W. J. Evans, and A. K. McMahan, Phys. Rev. Lett. **101**, 165703 (2008).
[16] J. F. Riecken, W. Hermes, B. Chevalier, R.-D. Hoffmann, F. M. Schappacher, and R. Pöttgen, Z. Anorg. Allg. Chem. **633**, 1094 (2007).
[17] J. A. Mydosh, A. M. Strydom, M. Baenitz, B. Chevalier, W. Hermes, and R. Pöttgen, Phys. Rev. B **83**, 054411 (2011).
[18] S. F. Matar, J. F. Riecken, B. Chevalier, R. Pöttgen, A. F. Al Alam, and V. Eyert, Phys. Rev. B **76**, 174434 (2007).
[19] R. Feyerherm, E. Dudzik, S. Valencia, J. A. Mydosh, Y.-K. Huang, W. Hermes, and R. Pöttgen, Phys. Rev. B **85**, 085120 (2012).
[20] O. N. Carlson and F. A. Schmidt, J. Less-Common. Met. **53**, 73 (1977).
[21] J. Rodriguez-Carvajal, Physica B **192**, 55 (1993).
[22] G. M. Sheldrick, Acta Crystallogr. Sect. A **64**, 112 (2007).
[23] M. Rotter, H. Müller, E. Gratz, M. Doerr, and M. Loewenhaupt, Rev. Sci. Instrum. **69**, 2742 (1998).
[24] K. A. Gschneider, R. O. Elliott, and R. R. McDonald, J. Phys. Chem. Solids **23**, 555 (1962).